ACS APPLIED POLYMER MATERIALS

pubs.acs.org/acsapm

Article

Manganese(II)-PyNHC Complex as Visible-Light-Triggered Photocatalyst for Photopolymerization of Acrylates and 3D Printing

Camila Bignardi, Naralyne M. Pesqueira, Yasmin M. Shimizo, Antonio E. H. Machado, Diesley M. S. Araújo, Otaciro R. Nascimento, Valdemiro P. Carvalho, Jr., Jacques Lalevée,* and Beatriz E. Goi*

Cite This: *ACS Appl. Polym. Mater.* 2025, 7, 7429−7439

Read Online

ACCESS | Metrics & More | Article Recommendations | Supporting Information

ABSTRACT: Transition metals from the first series have recently attracted attention as potential photocatalysts in photopolymerization reactions and 3D printing applications. However, manganese(II) complexes are among the least explored in photopolymerization reactions. Hence, in this study, an organomanganese complex was developed bearing two pyridine-NHC ligands. The complex $[Mn^{II}(PyImes)_2](PF_6)_2$ (**Mn-PyImes**), where PyImes = *N*-mesityl-*N*′-2-pyridylimidazolium, was isolated upon heating a tetrahydrofuran (THF) solution of $MnCl_2$ with a 2-fold excess of $PyImes(PF_6)$ in the presence of potassium *tert*-butoxide (KO*t*Bu). **Mn-PyImes** was characterized by FTIR, UV−vis, fluorescence (steady state and time-resolved), and ESR spectroscopies, elemental analysis, cyclic voltammetry, and mass spectrometry. **Mn-PyImes** was applied in the reactions of controlled radical photopolymerization (CRP2) and free radical photopolymerization (FRP). **Mn-PyImes** showed slight control in the CRP2 of methyl acrylate (MA) using triethylamine (TEA) and phenacyl bromide (PhBr) as additives under LED@365 and LED@390−405. **Mn-PyImes** also showed a good catalytic ability in the FRP of ethoxylated trimethylolpropane triacrylate (TMPETA) under LED@405 nm, LED@455 nm, and laser diode@532 nm using di-*tert*-butyldiphenyl iodonium hexafluorophosphate (Iod) and ethyl dimethylaminobenzoate (EDB) as additives in a photoinitiating system. The CRP2 chemical mechanism was studied by electron spin resonance spin trapping, fluorescence, cyclic voltammetry, laser flash photolysis, and steady state photolysis techniques. Although **Mn-PyImes** demonstrated good light absorption properties under LED@365 nm, it also enabled effective photopolymerization of acrylates in thick films upon exposure to LED@405 nm, LED@455 nm, and laser diode@532 nm. More interestingly, stereoscopic 3D patterns were successfully fabricated by the laser writing technique.

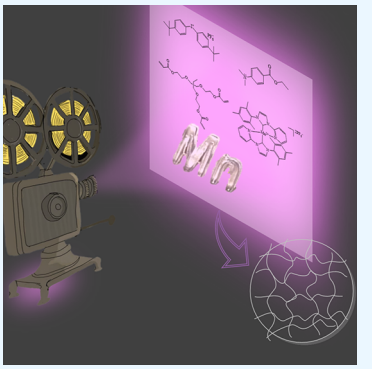

KEYWORDS: *Photopolymerization, Organomanganese(II), NHC, Photocatalysis, DLW*

1. INTRODUCTION

Since the past decade, there is an increasing interest in 3*d* metal complexes for their magnetic, optical, and charge transfer properties, particularly as cost-effective alternatives to second- and third-row transition metals in luminescent compounds for advanced technology.[1−4] Manganese has natural abundance and useful features of being a nontoxic and biocompatible metal.[5] Most complexes of manganese described in the literature feature the metal in oxidation states +1 and +2. Among the various valence states of the manganese ion, the divalent Mn(II) ion, with a $3d^5$ electron configuration, is especially notable for its well-defined $^4T_1-^6A_1$ radiative transition. This transition is closely linked to the strength of the crystal field, which alters the splitting of the *d*-orbitals and thus impacts the optical properties of the complex. These properties make Mn(II) complexes highly relevant in fields such as luminescent materials, magnetic applications, and charge-transfer-based technologies.[5−12]

Organomanganese(II) compounds are significantly more stable than most organometallics derived from transition metals, allowing frequent use at room temperature.[6] The organometallic chemistry of Mn(II) is distinguished by a significant ionic character in the Mn(II)−C bonds. Manganese carbene complexes are important due to their applications in organic synthesis, synthetic methodology, and theoretical implications.[6,7] Despite their potential, however, this family of complexes remains relatively underexplored in catalysis or photocatalysis. Only a few works have reported the organomanganese(II) complexes as catalysts; some of them are illustrated in Scheme 1. With their promising features, further exploration of Mn(II)−C complexes in catalytic

Received: March 25, 2025
Revised: May 24, 2025
Accepted: May 25, 2025
Published: June 4, 2025

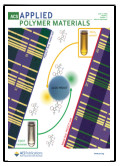

Scheme 1. Illustration of Catalysts Based on the Mn(II)-NHC System

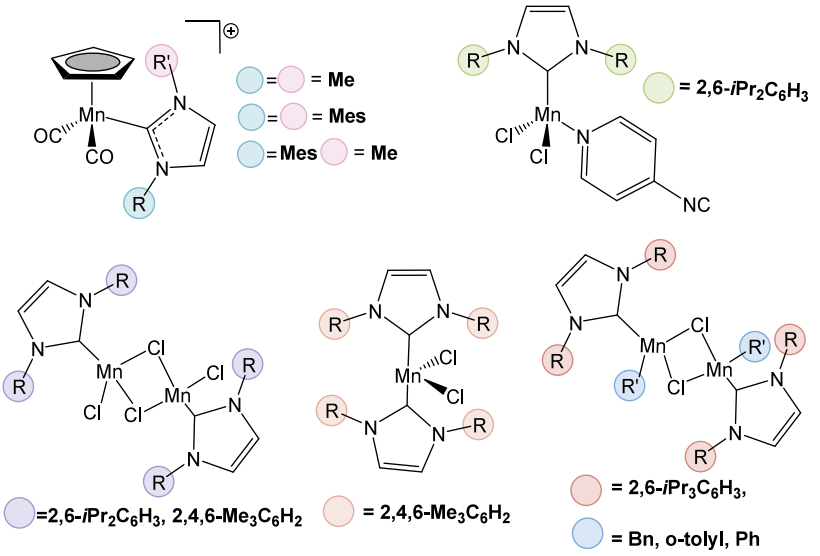

Scheme 2. Photocatalyst, Additives, and Monomers Used in Photopolymerization Reactions

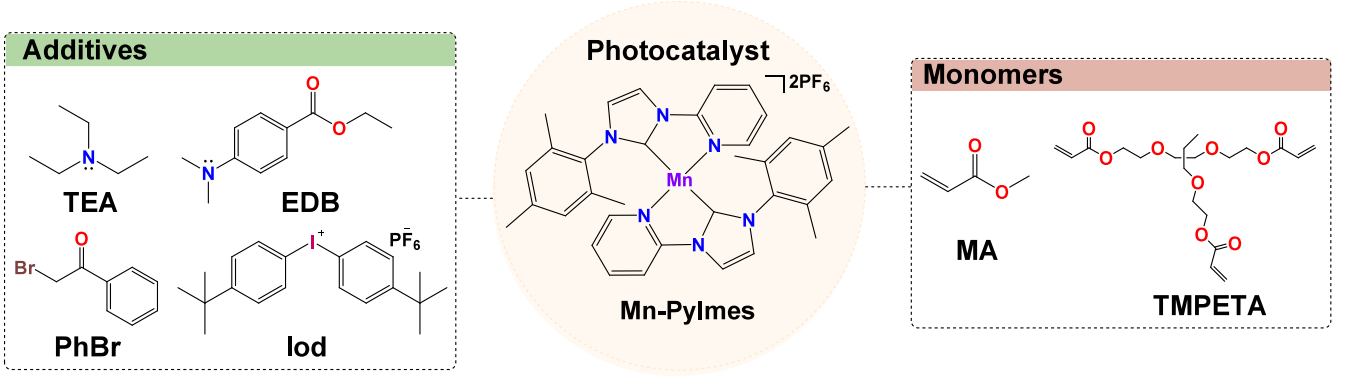

applications could unlock new possibilities in synthetic chemistry.[9,13]

The chemistry of N-heterocyclic carbenes (NHCs) has advanced significantly over the past few decades due to their unique role in stabilizing metal complexes and facilitating catalytic processes. By modifying their structure, NHC ligands can be tailored to optimize steric and electronic properties, enhancing their σ-donating and π-accepting abilities to influence the reactivity of coordinated metal centers.[14−16] Given their versatility and tunable properties, NHC ligands have also found utility in various photopolymerization processes.[17−19] In this regard, both controlled radical photopolymerization (CRP2) and free radical photopolymerization (FRP) can benefit from the unique characteristics of imidazolidine derivates.[20,21] The metal-based catalysts with NHC ligands have been extensively studied for wide applications of their luminescent properties, particularly silver, gold,[22−24] iridium,[25,26] ruthenium,[27,28] copper,[29,30] and rhenium.[31,32] complexes. CRP2 represents a powerful strategy that combines the spatial and temporal precision of light activation with the molecular control of reversible deactivation radical polymerizations. That is, the dormant species can be specifically (re)activated upon light irradiation. This approach enables the synthesis of polymers with well-defined architectures and narrow dispersities under mild conditions. CRP2 methodologies are particularly attractive for advanced manufacturing techniques, including 3D printing and microfabrication, where precision and functional tunability are essential.[33]

To evaluate the photoinitiation efficiency of manganese-based photoinitiating systems (PISs) in CRP2 and FRP under LED irradiation, a novel manganese(II)-NHC complex featuring an asymmetric ligand was synthesized. This complex was investigated as a photocatalyst within a three-component system containing acrylate monomers (MA, methyl acrylate; or TMPETA, ethoxylated trimethylolpropane triacrylate), with various additives used as oxidizing or reducing agents (i.e., amines, phenacyl bromide, or iodonium salt) (Scheme 2). The proposed photopolymerization mechanism was examined through cyclic voltammetry, electron spin resonance (ESR) spin trapping, and steady-state photolysis. Notably, 3D patterns were fabricated by direct laser writing, demonstrating the efficiency of the manganese(II)-NHC complex as a photocatalyst.

2. EXPERIMENTAL SECTION

2.1. General Remarks. All reagents were purchased from Aldrich Chemical Co. All reactions and manipulations were performed under a nitrogen atmosphere using standard Schlenk techniques. Methyl acrylate (MA) was washed three times with a 5% NaOH solution at an equimolar ratio. Subsequently, CaH_2 was added, and the system was agitated for 24 h. After that, the monomer was distilled from

https://doi.org/10.1021/acsapm.5c00982
ACS Appl. Polym. Mater. 2025, 7, 7429−7439

CaH_2, dried over anhydrous $MgSO_4$, and stored at −18 °C under nitrogen. 2-Bromopyridine, 2,4,6-trimethylaniline, formaldehyde, phenacyl bromide (Ph-Br), di-*tert*-butyl-diphenyl iodonium hexafluorophosphate (Iod), ethyl 4-(dimethylamino)-benzoate (EDB), ethoxylated (3) trimethylolpropane triacrylate (TMPETA), and triethylamine (TEA) were used without further purification. The ligand 3-(2-pyridinyl)-1-(2,4,6-trimethylphenyl)-1*H*-imidazolium hexafluorophosphate (PyImes) was synthesized as reported in the literature,[34,35] and its purity was confirmed by spectroscopic methods; details are provided in the Supporting Information (Figures S1−S4).

2.2. Analyses. Infrared spectra were obtained on a PerkinElmer Frontier instrument equipped with a diamond ATR module, recording between 4000 and 250 cm^{-1} at a scan rate of one spectrum per 64 s with 2 cm^{-1} resolution, at 298 K. The ^1H and $^{13}C\{^1H\}$ NMR spectra were recorded in $CDCl_3$ at 298 K on an Agilent MR 400 Ultrashield spectrometer operating at 400.13 and 100.61 MHz, respectively. Chemical shifts are reported in parts per million relative to the high frequency of tetramethylsilane (TMS). ESR measurements were performed in a Varian X-band EPR (model E-109). The measurements were conducted at two temperatures, 295 and 77 K, under the following EPR conditions: microwave frequency of 9.270 GHz, 100 kHz field modulation using an amplitude of 1.0 mT, 5 mW of microwave power, gain set to 1000, center field at 410 mT, scan range of 800 mT, time constant of 0.064 s, and scan field collecting 4096 points over 4 min. The ESR spectra were simulated with the EasySpin program. UV−vis measurements were performed on a Shimadzu UV-2600 UV−vis spectrophotometer with 1 cm path length quartz cells. CH_2Cl_2 solutions of the complexes at 0.5 mmol L^{-1} concentration were used for these measurements. The MALDI-TOF was acquired in a MALDI Autoflex Max equipment with a positive reflector mode. The sample was mixed with the matrix HCCA (α-cyano-4-hydroxycinnamic acid 10 mg mL^{-1} in 50% CH_3CN + 0.1% TFA) with the proportion 1:1 (v/v). Electrochemical measurements were performed by employing an Autolab PGSTAT204 potentiostat equipped with a stationary platinum disk as the working electrode and a wire as the auxiliary electrode. The reference electrode utilized was Ag/AgCl. The measurements were conducted at 25 °C ± 0.1 in CH_3CN with 0.1 mol L^{-1} of *n*-Bu_4NPF_6. The fluorescence measurements were performed in an RF6000 Shimadzu in CH_2Cl_2 solutions of 2.0×10^{-4} mol L^{-1}. Fluorescence excited-state lifetimes were determined with a HORIBA PPD-850 detector. The impulse response function (IRF) of the apparatus was evaluated through the colloidal silica suspension LUDOX, and the excitation wavelength was set at 367. The residual monomer concentration, which determined the monomer conversion, was measured by infrared spectra using a PerkinElmer Frontier instrument equipped with a diamond ATR module. Molecular weights and the molecular weight distribution of the polymers were determined by gel permeation chromatography using a Shimadzu Prominence LC system equipped with an LC-20AD pump, a DGU-20A5 degasser, a CBM-20A communication module, a CTO-20A oven at 40 °C, and a RID-10A detector, equipped with two Shimadzu columns (GPC-805:30 cm, Ø = 8.0 mm). Retention times were calibrated with monodispersed poly(methyl methacrylate) standards in HPLC-grade THF as an eluent at 40 °C with a flow rate of 1.0 mL min^{-1}. The dispersity index (*Đ*) is defined as M_w/M_n. Electron spin resonance spin trapping (ESR-ST) experiments were conducted using an X-band spectrometer (Bruker EMXplus) under an LED@365 and 390−405 nm. The generated radicals were captured using 5,5-dimethyl-1-pyrroline-*N*-oxide (DMPO) in CH_2Cl_2. For laser flash photolysis experiments, a Luzchem LFP 212 setup was used: a Q-switched nanosecond (Nd/YAG) laser (λ_{exc} = 355 nm, 9 ns pulses) (Continuum Minilite) was used for the excitation, and the analyzing system consisted of a ceramic xenon lamp, a monochromator, a fast photomultiplier, and a transient digitizer.

2.4. Synthesis of $[Mn^{II}(PyImes)_2](PF_6)_2$ (Mn-PyImes). The $MnCl_2$ (0.6 mmol, 1.0 equiv), py-Imes(PF_6) (1.3 mmol, 2.2 equiv), and KO*t*Bu (1.5 mmol, 2.5 equiv) were added in a 25 mL Schlenk tube under an inert nitrogen atmosphere. Subsequently, 15 mL of THF was added to the reaction mixture. The reaction was then allowed to proceed with stirring at 40 °C for 24 h using a heating mantle. Upon completion of the reaction, the mixture was cooled to room temperature. Excess THF was removed under reduced pressure to concentrate the reaction mixture, and hexane was added to precipitate the product. The resulting crude product was subjected to ethanol washes to remove unreacted ligand and $MnCl_2$. The pale-brown solid obtained after filtration was dried under a vacuum, yielding the desired compound. Yields: 45%, (0.235 g). (a) FTIR (cm^{-1}): ν(C−H) 3118−2993, ν(C═N) 1604, ν(C═C) 1618, $\nu(PF_6)$ 842 and 558, ν(Mn−N) 417. (b) UV−vis $\lambda_{max(n)}$ (nm), $\varepsilon_{max(n)}$ ($M^{-1}c\ m^{-1}$): $\lambda_{max(1)}$ 240, $\varepsilon_{(1)}$ 1802; $\lambda_{max(2)}$ 275, $\varepsilon_{(1)}$ 1932; $\lambda_{max(3)}$ 316, $\varepsilon_{(3)}$ 1409; (c) Anal. Calculated for $C_{34}H_{34}MnN_6P_2F_{12}$: C, 46.75; H, 4.15; N, 9.62 (%); found: C, 46.92; H, 4.22; N, 9.82. (d) MALDI-TOF: *m*/*z* calcd for $C_{34}H_{34}F_{12}N_6MnP_2$: 290.6100 g mol^{-1}; found: 290.8218 ($[M - 2PF_6^-]^{2+}$).

2.5. General Procedure for Photopolymerization Reactions. Bulk polymerizations of methyl acrylate (MA) were monitored in real time with an FTIR spectrophotometer (PerkinElmer Frontier). The formulations were prepared mixing the **Mn-PyImes**, phenacyl bromide (Ph-Br), triethylamine (TEA), and MA at different molar ratios. The sample was injected into a circular mold that was placed on a sample holder in the ATR module. A real-time Fourier transform infrared spectrometer (RT-FTIR) was used to follow the C═C double-bond conversion (for acrylate functionality) versus time for polymerizations. The decrease of the C═C bond at 1635 cm^{-1} was followed. LED@365 and LED@390−405 nm having an intensity of 10 mW/cm^2 at the sample position were used for the photopolymerization experiments. The reinitiation experiments under light irradiation were also studied.

2.6. Direct Laser Writing (DLW). Direct laser writing experiments were conducted using a computer-controlled laser diode at 405 nm ($I_0 \approx 110$ mW) with a spot size of 50 μm to inscribe specific 3D patterns in air from the monomer TMPETA, incorporating the proposed three-component system (Mn/Iod/EDB). The formulation was deposited in a custom-made glass tank with a resin layer of 2.2 mm. The resulting patterns (letters) were created through the polymerization of the formulation and analyzed using a numerical optical microscope (DSX-HRSU from the Olympus Corporation).

3. RESULTS AND DISCUSSION

3.1. Synthesis and Characterization. Few studies have reported the synthesis of Mn(II)-NHC complexes. In 2004, Noltemeyer et al. reported three new manganese(II) complexes bearing two NHC ligands $[MnX_2(C\{N(iPr)C(Me)\}_2)_2]$ [X = Cl; I; MeCOO] using different MnX precursors.[36] More recently, Tonzetich and co-workers reported a series of manganese(II) complexes[9] with the structure $[Mn_2(\mu\text{-}Cl)_2(NHC)_2]$ using $MnCl_2$ as the precursor in the presence of THF as solvent at room temperature. NHC-based ligands are typically complexed with metallic centers under moisture- and oxygen-free conditions due to the high reactivity of the carbenes. The most common method involves direct coordination of the free carbene, either via a one-pot procedure or through a stepwise approach. Bases like *n*-BuLi, NaH, KO*t*Bu, Cs_2CO_3, or KHMDS are used to deprotonate the azolium precursor. Regarding this information, the synthesis of the **Mn-PyImes** was conducted relying on similar procedures for NHC-based manganese, cobalt,[37] and iron[38] complexes. Here in this paper, KO*t*Bu, Cs_2CO_3, or KHMDS was tested, with the KO*t*Bu being the best base for the reaction reported, with higher yields. In a typical experiment, the $MnCl_2$ (1 equiv) and a small excess of *py*-Imes·PF_6 (2.2 equiv) and KO*t*Bu (2.5 equiv) were stirred in dry THF for 24 h at 40 °C to lead to the formation of **Mn-PyImes** (Scheme S1). The complex was isolated by recrystallization from CH_2Cl_2/hexane and washed with ethanol as a pale-brown powder. This thermal

https://doi.org/10.1021/acsapm.5c00982
ACS Appl. Polym. Mater. 2025, 7, 7429−7439

treatment was required to achieve a better yield of pure product.

Mn-PyImes was characterized by elemental analysis, FTIR, UV−vis, fluorescence, and EPR spectroscopies, mass spectrometry, and cyclic voltammetry. The elemental analysis data of **Mn-PyImes**, listed in the Experimental Section, are compatible with the theoretical values, suggesting the formation of the **Mn-PyImes** complex. The MALDI-TOF spectrum of **Mn-PyImes** exhibits the molecular ion peak m/z at 290.8218, which agrees well with the suggested molecular formula derived from elemental analysis (Figure S5). The infrared spectrum of the **Mn-PyImes** shows a band around 2944−2807 cm^{-1} referring to the asymmetric and symmetric stretching modes of ν(C−H), whereas these bands are observed in a higher wavenumber in the free *py*-Imes ligand, around 2734−2662 cm^{-1} (Figure S6). For the free *py*-Imes ligand, an intense absorption band is observed at 1615 cm^{-1}, assigned to the ν(C═N) vibration of the pyridine moiety. After coordination, this ν(C═N) absorption band was shifted to lower frequencies (1604 cm^{-1}), compared to the free *py*-Imes ligand. These results agree with the change in the electronic density of these groups after the coordination of the *py*-Imes ligand to the manganese center, which occurred in a bidentate N_{Py}^C_{NHC}-cyclometalated mode.[13,38] The bands at 842 and 558 cm^{-1}, observed in both **Mn-PyImes** and free *py*-Imes ligand infrared spectra, are attributed to the PF_6^- counterion.[39] Moreover, the ν(Mn−N) stretching vibration occurs as a very weak band in a low-intensity region at 417 cm^{-1}.[8,40,41] ESR spectra of **Mn-PyImes** are shown in Figure S7 in frozen CH_2Cl_2 solution at both 295 and 77 K. The behavior found in the spectra is that typically found for Mn^{II} d^5, which favors a high-spin state of $S = 5/2$, arising from the central transition of $M_S = -1/2$ to $+1/2$, with $g \approx 2$. The spectra show nuclear hyperfine interaction, with the six lines corresponding to the Mn nuclear spin ($I = 5/2$). These data suggest that **Mn-PyImes** has a highly distorted tetrahedral geometry.[42]

The optimized geometry for **Mn-PyImes** (Figure S8) was obtained by DFT using the M06 functional[43] in combination with the Jorge-TZP-DKH basis set.[44,45] This calculation was performed by considering this molecule solvated in dichloromethane. For this, the dielectric continuous model CPCM was used.[46,47] Electronic excitation spectra for the first 50 excited singlet states of the solvated compound were obtained using TD-DFT calculation, employing a combination between the hybrid functional CAM-B3LYP[48] and the atomic basis set dgdzvp2. All calculations were performed using the Gaussian version G09, revision E1.[49] Selected bond distances and bond angles from these calculations are listed in Table S1. The bond angles that are diagnostic are 158.059°, 70.569°, 100.534°, 95.900°, and 79.754°, respectively, for C(1)−Mn−C(2), C(1)−Mn−N(1), C(1)−Mn−N(2), N(1)−Mn−N(2), and C(2)−Mn−N(2). These angles, along with the bond lengths, are consistent with values reported for analogous manganese-(II) complexes,[50] indicating a distorted tetrahedral geometry around the metal center. This structural arrangement is further supported by ESR data, which confirm the presence of a high-spin Mn(II) ion. The *py*-Imes ligands are coordinated in a bidentate cyclometaled mode through the nitrogen atom of the pyridine group and the carbon atom of the imidazole ring. This coordination forms two five-membered chelate rings that exhibit significant electron density delocalization.

The UV−vis spectrum in CH_2Cl_2 solution (5×10^{-4} mol L^{-1}) for **Mn-PyImes** is characterized by high-energy bands around 240−320, which can be assigned to ligand localized, intraligand $\pi-\pi^*$ and $n\rightarrow\pi^*$ transitions (Figure S9). Moreover, **Mn-PyImes** exhibits a lower-energy band spanning 360−500 nm, which can be assigned as ligand-to-metal charge transfer (LMCT) transitions from the *py*-Imes ligand to the Mn center.[50]

The absorption peaks of **Mn-PyImes** were assigned based on time-dependent DFT (TD-DFT) in CH_2Cl_2 solution (Figure 1). For **Mn-PyImes**, the peaks observed at 212 and

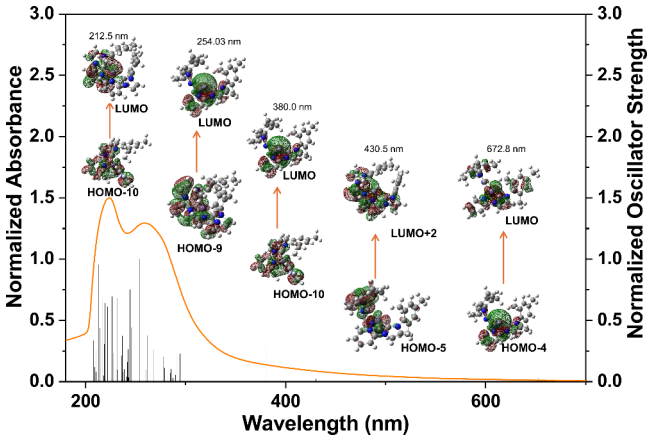

Figure 1. UV−vis experimental and theoretical spectra of **Mn-PyImes** in CH_2Cl_2 at 25 °C; [Mn] = 5×10^{-4} mol L^{-1}.

254 nm have IL character corresponding to HOMO−6 → LUMO+3, HOMO−8 → LUMO+2, HOMO−8 → LUMO +1, HOMO−10 → LUMO+1 and HOMO−6 → LUMO+3, HOMO−8 → LUMO+2, HOMO−8 → LUMO+1, HOMO−10 → LUMO+1 transitions, respectively, with a contribution of 98−90% of the *py*-Imes orbitals. The calculated transition at 380.47 nm is predominantly LMCT (54%) character corresponding to HOMO−8 → LUMO, HOMO−9 → LUMO, and HOMO−10 → LUMO transitions but also shows IL and MLCT contributions (30%). Another two transitions at 430.15 and 652.40 nm can be configured as discrete MLCT, corresponding to HOMO−5 → LUMO+2, HOMO−5 → LUMO+3, HOMO−5 → LUMO+6, HOMO−4 → LUMO+2 and HOMO−4 → LUMO, HOMO−4 → LUMO+1, HOMO−4 → LUMO+4, HOMO−4 → LUMO +6, respectively.

As shown in Figure S10, the emission spectrum of **Mn-PyImes** recorded in CH_2Cl_2 solution with an excitation wavelength of 365 nm reveals a band with a maximum of 424−454 nm, indicating that **Mn-PyImes** is capable of fluorescence emission in the blue region. Additionally, the strong σ-donating nature of NHC ligands can significantly improve the luminescent properties of metal complexes.[50] This effect raises the energy levels of nonradiative metal-centered (MC) $d-d$ transitions, thus enabling the formation of emissive Mn(II) complexes. Regarding the lifetime in the singlet state, **Mn-PyImes** displays a lifetime (τ) of 3.25 ns, as shown in Figure S11. No additional transient species are formed when **Mn-PyImes** is irradiated at 355 nm in laser flash photolysis experiments. To gain insight into the luminescence properties of **Mn-PyImes**, solvent effect experiments were conducted in solvents of varying polarity. Thus, the emission of the complex was investigated in CH_2Cl_2, ethyl acetate, DMF, and CH_3CN upon excitation at 365 nm (Figure S12). Upon increasing

https://doi.org/10.1021/acsapm.5c00982
ACS Appl. Polym. Mater. 2025, 7, 7429−7439

solvent polarity, the emission band shifted to longer wavelengths, demonstrating solvatochromism properties. Moreover, the highest emission band was observed in CH_2Cl_2, a solvent with lower polarity compared to the other solvents investigated. Interestingly, **Mn-PyImes** exhibited lower emission and a shift from 424 to 460 nm in the presence of DMF and CH_3CN compared to CH_2Cl_2, which can be associated with the coordinating nature of these solvents. The excited energy was calculated and found to be 3.4 eV for **Mn-PyImes** (Figure S13).

3.2. Controlling Ability of Mn-PyImes in the MA Photopolymerization. In order to investigate the behavior of **Mn-PyImes** as photocatalyst in photopolymerization reactions, it has been studied in several conditions, as can be seen from Table S2 and Table 1. Photopolymerization of MA performed

Table 1. MA Photopolymerization Conditions under LED@390−405 nm, at Room Temperature in the Presence of PhBr, TEA, and Mn Complex

Entry	MA/Mn^{II}/ PhBr/ TEA	Conversion (%)	Induction time (s)	Mn (g mol^{-1})	$Đ$
1	200/0.02/1/1	68	20	72 000	1.7
2	200/0.02/0.5/0.5	65	100	59 700	1.6
3	200/0.02/1/0.75	76	60	99 000	2.1
4	200/0.02/2/2	80	30	38 000	2.9
5	400/0.02/1/1	8	300	117 000	1.8
6	200/0.2/1/1	76	60	116 000	1.6
7	200/0/1/1	77	10	40 000	2.9
8	200/0.02/1/0	-	-	-	-
9	200/0.02/0/1	-	-	-	-
10	200/0/1/0	-	-	-	-
11	200/0/0/1	-	-	-	-
12	200/0.1/0.5/0.5	42	60	150 000	1.4
13	200/0/0.5/0.5	74	10	260 000	2.7

in the RT-FTIR using the **Mn-PyImes**/PhBr/TEA PIS was carried out at LED@365 and LED@390−405 nm irradiation. **Mn-PyImes** exhibits a slight UV/visible light absorption that can be interesting upon violet LED irradiation. Indeed, with the ε of the **Mn-PyImes** at the wavelength delivered by the LED@365 and LED@390−405 nm, the photopolymerization experiments were suitable ($\varepsilon_{365\ nm}$ = 494, $\varepsilon_{390\ nm}$ = 381, and $\varepsilon_{405\ nm}$ = 345 M^{-1} cm^{-1}, respectively). After the irradiation, the samples were solubilized in THF and analyzed by SEC. PMA polymers were obtained with poor control of the polymer chains.

The photopolymerization reactions performed under an LED@365 nm are displayed in Table S2. The preliminary tests were conducted in (i) the absence of light, in which no polymerization occurred; (ii) Mn complex and an MA system (entry 9, Table S2), where no polymers were formed; (iii) PhBr/MA (entry 10, Table S2), in which the polymerization reached a conversion of 80% and $Đ$ = 2.5; (iv) TEA/MA (entry 11, Table S2), where no polymerization was seen; (v) PhBr/Mn/MA (entry 8, Table S2), where the polymer formed reached 85% conversion and $Đ$ = 2.0; (vi) PhBr/TEA/MA (entry 7, Table S2), in which the polymerization reached the highest conversion (92%) and $Đ$ = 2.5.

The resulting photopolymerization profiles under LED@365 nm are presented in Figure S14, monitored for up to 300 s, and SEC curves are in the Supporting Information (Figure S15). In the molar ratio of 200/0.02/1/1, no inhibition time was observed, indicating that radical generation occurred immediately upon initiation of the reaction (entry 1, Table S2). Interestingly, when the concentration of TEA decreased from 1 to 0.75 (entry 3, Table S2), a lower conversion rate and a slower polymerization rate were observed, as shown in Figure S15 and Table S2 (entries 1−3). A similar trend is evident when entries 1 and 2 (Table S2) are compared. With lower concentrations of both TEA and PhBr, the reaction proceeds more slowly, resulting in reduced conversion within 300 s (Figure 5). However, when the concentration of additives was

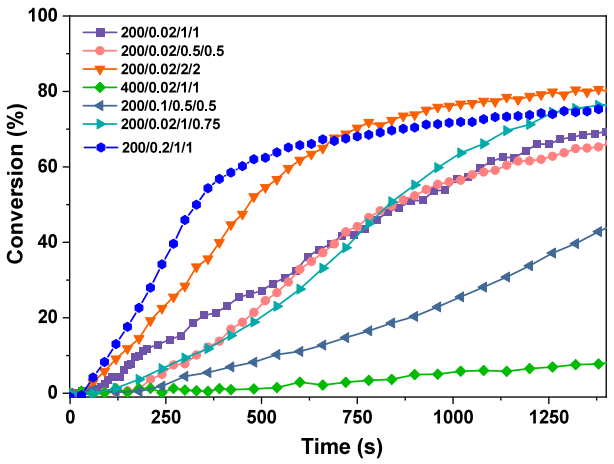

Figure 2. Photopolymerization profiles of MA (acrylate function conversion vs irradiation time) initiated by PhBr/Mn^{II}/TEA-based three-component PISs upon irradiation with LED@390−405 nm in bulk, with different conditions.

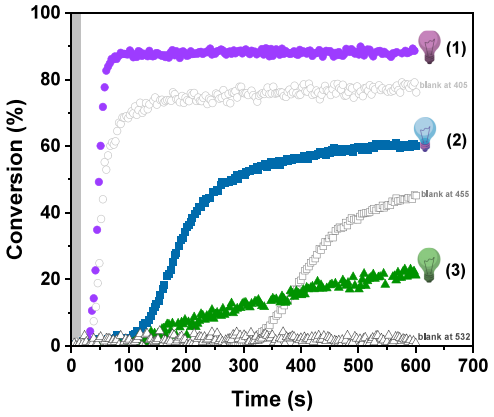

Figure 3. Photopolymerization profiles of TMPETA (acrylate function conversion vs irradiation time) initiated by PC/Iod/EDB in the ratio of 2%/2%/2% based three-component PISs upon irradiation with LED@405 (1, ●), 455 (2, ■), and laser@532 nm (3, ▲) in bulk at room temperature under air. PC = **Mn-PyImes**.

increased (entry 4, Table S2), polymerization was accelerated, achieving 78% conversion within 210 s due to enhanced radical propagation. A comparison of entries 1 and 5 (Table S2) indicates that increasing the MA ratio slows the polymerization rate while resulting in an 82% conversion. Finally, with increased [Mn^{II}] (entry 6, Table S2), a slower polymerization profile was observed, reaching a conversion of 47%.

The photoinitiating ability for **Mn-PyImes** was also evaluated under LED@390−405 nm (Table 1). The use of LED@390−405 nm led to a difference in the photo-

https://doi.org/10.1021/acsapm.5c00982
ACS Appl. Polym. Mater. 2025, 7, 7429−7439

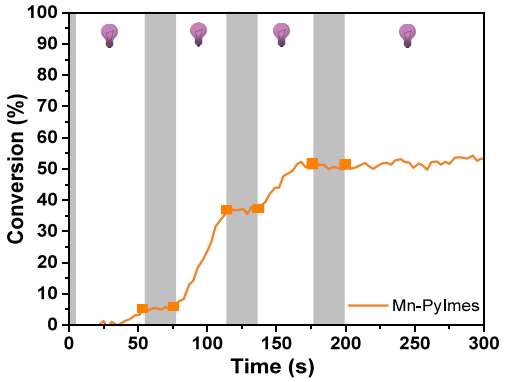

Figure 4. On−off photopolymerization profile of TMPETA using the **Mn-PyImes**/Iod/EDB (0.2%/2%/2% w/w) PIS; irradiation: LED@405.

polymerization profiles, as can be seen in Figure S16. The condition monitored was using a molar ratio MA/PhBr/Mn/TEA = 200/1/0.02/1 in both LEDs until 600 s. Interestingly, the photopolymerization under 365 nm irradiation was faster due to higher absorption by the **Mn-PyImes** and the charge transfer complex formed by TEA and PhBr.[50,51] However, when comparing the dispersity ($Đ$) of the polymers, the reaction at 390−405 nm resulted in slightly more controlled polymerization ($Đ$ = 1.7) compared to those at 365 nm ($Đ$ = 2.1) in the molar ratio of 200/0.02/1/1 (Table S2, entry 1, and Table 1, entry 1). These findings indicate that while higher wavelengths lead to slower polymerization, they may provide improved control over the polymerization process.

Control experiments in LED@390−405 nm revealed that omission of any single component—whether **Mn-PyImes**, PhBr, TEA, or the light source—resulted in no polymeric product formation (entries 8−11, Table 1). All the photopolymerization conditions exhibited an inhibition time, ranging from 10 to 100 s, as shown in Table 1.

The polymerization profiles, as illustrated in Figure 2, reveal key trends in conversion and dispersity under different conditions; the SEC curves are in the Supporting Information (Figure S17). The molar ratio of 200/0.02/1/1 entry 1 (purple) reaches a plateau at 68% conversion after 1400 s with a slightly controlled profile ($Đ$ = 1.7, entry 1, Table 1). These results showed that $M_{n,exp}$ decreased from about 72 000 to 38 000 g mol^{-1} and the $Đ$ was increased to 2.9 with an increase in the additive concentration (entry 4, Table 1). When the additive concentration was decreased (entry 2, Table 1), both the $M_{n,exp}$ and the $Đ$ were decreased ($M_{n,exp}$ = 59 700 g mol^{-1} and $Đ$ = 1.6) and conversion was reduced (65%). The lower additive concentration also slowed radical production, as indicated by an inhibition time of 100 s (entry 2, Table 1). Interestingly, if only the TEA is decreased, the system becomes faster, reaching 76% conversion with decontrolled polymer chains (entry 3, Table 1). This study highlights the critical role of additive concentration in modulating polymerization speed, conversion, and the control of polymer chain properties. Also, the behavior of **Mn-PyImes** can be evidenced when entries 1 and 6 (Table 1) are compared: the increase in the Mn ratio improved the conversion from 68% (entry 1, Table 1) to 76% (entry 6, Table 1) with a higher inhibition time (40 s more than for entry 1), but with lower $Đ$ values ($Đ$ = 1.7 for entry 1 and $Đ$ = 1.6 for entry 6, Table 1). For all the conditions in the presence of Mn^{II} an increase in the conversion values and a decrease in the $Đ$ can be observed, suggesting that the complex plays a role in controlling the photopolymerization of MA under 390−405 nm LED irradiation. The presence of the inhibition times is consistent with literature[22,54−56] and might be influenced by the O_2 diffusion, which causes inhibition in the radical photopolymerization, as well as the inner effect filter.

3.3. FRP of TMPETA. In order to evaluate the ability of the **Mn-PyImes** in 3D printing, experiments of FRP were conducted under LED@405 nm (I_0 ≈ 110 mW·cm^{-2} with an incident light intensity at the sample surface of I_0 ≈ 10 mW·

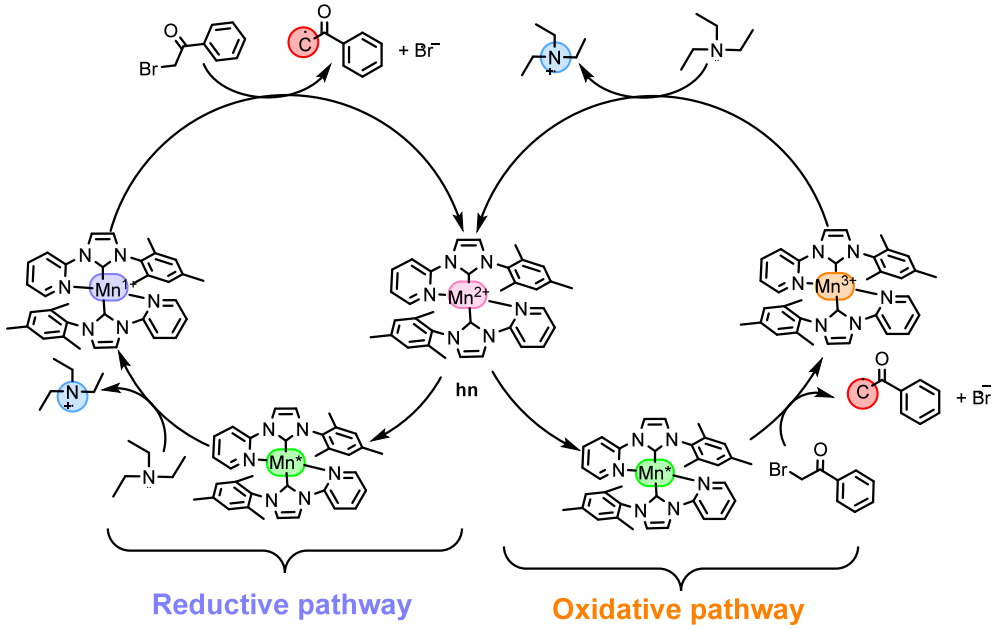

Figure 5. Proposed mechanism for the photopolymerization reactions in the presence of TEA and PhBr using **Mn-PyImes** as the catalyst under an LED@365 nm.

https://doi.org/10.1021/acsapm.5c00982
ACS Appl. Polym. Mater. 2025, 7, 7429−7439

cm^{-2}), in the presence of PC/Iod/EDB in the conditions 0.1%/1%/1%, 0.2%/1%/1%, and 0.2%/2%/2% in weight under air (2.0 mm thickness), as in the literature (Figure S18).[55] Iod and EDB correspond to usual redox agents in 3D printing photosensitive systems.[55,56] Comparing the curves of the blank and the PIS with those of **Mn-PyImes**, it is possible to observe the photocatalyst ability of the complex. For the blank with 1% of additives, the maximum conversion value was 69% within 200 s with an inhibition time of 50 s. In the presence of **Mn-PyImes**, the conversion reached 78% with an inhibition time decreasing to 60 s. Increasing the PC amount from 0.1% to 0.2% led to a reduction in the inhibition time to 30 s, while the conversion remained at 75%. Under a 2%/2% Iod/EDB ratio, the inhibition lasted 40 s, achieving 78% conversion within 600 s. However, with **Mn-PyImes** (curve 3), the inhibition time decreased to 10 s and the conversion increased to 88% within 100 s.

Based on the previous results and to gain a deeper understanding of the behavior of **Mn-PyImes**, the FRP of TMPETA was conducted in the presence of air using the optimal composition of 0.2%/2%/2% w/w/w Mn^{II}/Iod/EDB under different irradiation sources (LED@405 nm, LED@455 nm, and laser diode@532 nm) (Figure 3). At LED@405 nm, the final conversion reached was 88% with an inhibition time of 20 s, while the blank exhibited 78% with 30 s. According to the literature, the conversion of TMPETA using the blank is attributed to the CTC formed between EDB and Iod, which is active in the FRP under 405 nm irradiation and much less for longer wavelengths (less absorption).[52,53] Therefore, experiments for longer wavelengths better highlight the crucial role of role **Mn-PyImes**; that is, under LED@455 nm, a higher conversion (60%) and shorter inhibition time (40 s) are observed with **Mn-PyImes** compared to the blank (45% conversion and 300 s inhibition). Remarkably, the photopolymerization reaction with **Mn-PyImes** also proceeded under the green laser diode@532 nm, reaching 22% conversion after 600 s, whereas no polymerization occurred for the blank. Following these experiments, **Mn-PyImes** plays a crucial role in initiating polymerization under these conditions, demonstrating good catalytic activity under visible light irradiation in the presence of air.

Furthermore, the PIS PC/Iod/EDB in 0.2%/2%/2% was also applied in light on−off experiments by exposure to LED light with repeated cycles by switching the light on for 40 s and off for 20 s. As a result, polymerization was dependent on irradiation due to the lack of polymerization observed in the dark (Figure 4). The conversion obtained in the On−Off experiment was lower than in the continuous FRP experiment, which can be attributed to the formation of a polymer network with TMPETA. This behavior is likely influenced by diffusion-limited polymerization and the gel effect, where increased viscosity during polymerization restricts monomer mobility and radical propagation, leading to a reduction in overall conversion.[20,33]

3.4. Initiation Mechanism of CRP2 of MA. In order to evaluate the interactions between Mn^{II}/PhBr and Mn^{II}/TEA, photolysis experiments were conducted in CH_2Cl_2 at 25 °C under an LED@390−405 nm for different durations. First, the stability of **Mn-PyImes** was investigated under LED irradiation, showing no changes over various time intervals (Figure S19a). For Mn^{II}/PhBr, an increase was observed between 400 and 800 nm, indicating the formation of a photoproduct due to the interaction between Mn and the PhBr additive (Figure S19b). In contrast, a minimal decline was observed after 740 s in Figure S19c, indicating a poor interaction between Mn^{II} and TEA. These results suggest an oxidative pathway, attributed to the stronger interaction between the Mn(II) complex and PhBr compared to that of TEA.

Furthermore, the three-component system, Mn^{II}/PhBr/TEA, was evaluated over 1380 s, with an isosbestic point at 370 nm suggesting a redox reaction without any side reactions[20,22] (Figure S19d). Notably, there is an increase after 380 nm, indicating the generation of radicals to initiate photopolymerization. These carbon radicals were identified through ESR spin-trapping experiments under LED irradiation, as shown in Figure S20.

By means of cyclic voltammetry (Figure S21), the oxidation and reduction potentials of **Mn-PyImes** and the free energy ΔG_{et} could be determined. Values of the oxidation potentials were −1.07, 0.82, and 1.24, which can be attributed to the redox pairs $Mn^{II/I}$, $Mn^{III/II}$, and $Mn^{IV/III}$, respectively. Also, the values of the reduction potentials were also found as −1.25, 0.60, and 1.09 V regarding the redox couples $Mn^{II/I}$, $Mn^{III/II}$, and $Mn^{IV/III}$, respectively.[57] The oxidation process at around 2.01 V is attributed to the ligand PyImes. The free energy change ΔG_{et} for electron transfer between singlet-excited **Mn-PyImes** and the additives PhBr/TEA and Iod/EDB can be calculated from the classical Rehm−Weller equation: $\Delta G = E_{ox} - E_{red} - E^* + C$, where E_{ox}, E_{red}, E^*, and C are the oxidation potentials of the electron donor, the reduction potential of the electron acceptor, the excited singlet state of **Mn-PyImes**, and the electrostatic interaction energy of the initially formed ion pair, which is generally considered to be negligible in polar solvents.[58,59] The values are summarized in Table S3.

Remarkably, favorable fluorescence quenching processes of the excited singlet states by PhBr (Figure S22.a) are shown by the high value of the Stern−Volmer coefficients (K_{SV} = 69.3 L mol^{-1}), high electron transfer quantum yield (Φ_{et} = 0.79), and the favorable free energy changes (ΔG_{et}) for the expected electron transfer reaction between Mn and PhBr (ΔG_{et} = −3.37 eV). Also, the decrease in the emission intensity (I) after addition of the PhBr (Figure S22.a) confirmed quenching between the luminescent state of **Mn-PyImes** and PhBr. In contrast, minor interactions were observed between the Mn complex and TEA, as indicated by the lower K_{SV} value (21.6 L mol^{-1}), a moderate Φ value (0.53), and a less favorable ΔG_{et} value (−1.46 eV; Figure S22.b).

These results provide critical insights into the mechanistic pathways facilitated by the Mn(II) complex in the presence of TEA and PhBr, highlighting its ability to follow either an oxidative or a reductive pathway (Figure 5). First, the ground state of **Mn-PyImes** was converted to the excited state **Mn-PyImes*** under irradiation, and then the complex can react with PhBr or TEA in two different reactions. The oxidation reaction with PhBr could generate **Mn-PyImes**$^{3+}$, which can be reduced by TEA in the next step, regenerating **Mn-PyImes** in its initial state. On the other hand, the original form of **Mn-PyImes** also can be regenerated from **Mn-PyImes**$^{1+}$ to finalize the catalytic cycle when **Mn-PyImes**$^{1+}$ was oxidized by PhBr as well. However, based on the quenching experiments, photolysis results, and ΔG values, the oxidative pathway is the most favorable mechanism.

3.5. Direct Laser Writing. The FRP process of TMPETA could also be studied by its application in laser writing experiments under air using the **Mn-PyImes**-based three-

https://doi.org/10.1021/acsapm.5c00982
ACS Appl. Polym. Mater. 2025, 7, 7429−7439

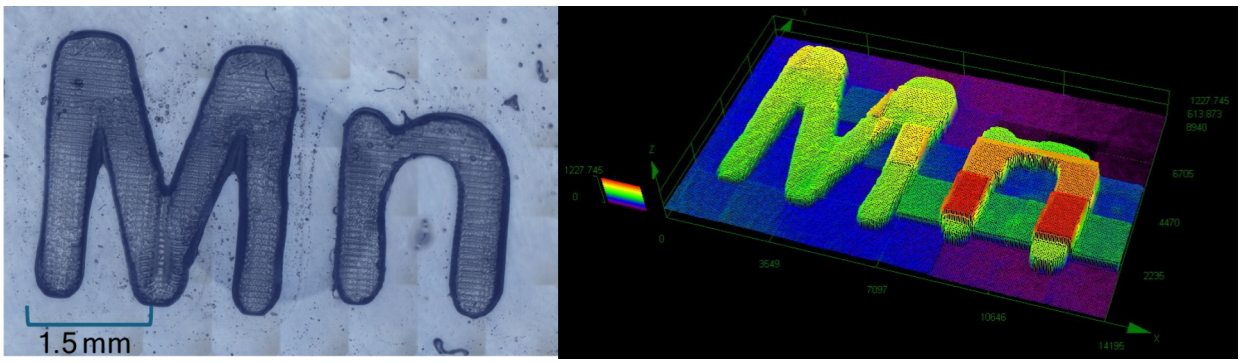

Figure 6. Photopolymerization experiments for laser writing initiated based three-component photoinitiating systems. Characterization of 3D overall appearance of color patterns determined by numerical optical microscopy in the presence of **Mn-PyImes**/Iod/EDB (0.2%/1%/1% in TMPETA, w/w/w).

component PIS (Mn/Iod/EDB, 0.2%/1%/1%, w/w/w) due to its high photosensitivity. As shown in Figure 6, the tridimensional patterns "Mn" could be fabricated successfully with excellent spatial resolution upon irradiation with a laser emitting at 405 nm. After that, further profilometric observation with a numerical optical microscope was used to characterize these letter patterns. All these results showed that writing with a remarkable spatial control was possible with the newly proposed PIS by laser writing experiments.

4.0. CONCLUSIONS

This study highlights the significant potential of the novel organomanganese(II) complex **Mn-PyImes** as a versatile photocatalyst in controlled radical photopolymerization (CRP2) and free radical photopolymerization (FRP). Comprehensive characterization using FTIR, UV−vis, MALDI-TOF, luminescence, and ESR spectroscopy revealed that **Mn-PyImes** exhibits green luminescence under UV irradiation, a singlet lifetime of 3.25 ns, and a tetrahedral geometry favoring a high-spin state ($S = 5/2$). The complex's redox behavior, with quasi-reversible $Mn^{2+}/^{3+}$ processes in CH_3CN, further underscores its electrochemical robustness. Photopolymerization studies demonstrated its catalytic efficiency under various light sources (LED@365, LED@390−405, and LED@405 nm), achieving high conversions in the polymerization of methyl acrylate (MA) and ethoxylated (3) trimethylolpropane triacrylate (TMPETA). The CRP2 of MA using TEA and PhBr yielded slightly controlled polymerization ($Đ < 2$) under LED@390−405 nm. In FRP, the complex facilitated the polymerization of TMPETA with high conversion under LED@405 nm, LED@455 nm, and laser diode@532 nm, showcasing its adaptability to different photopolymerization systems and different visible light irradiation sources. The On/Off experiment showed that polymerization was dependent on irradiation due to the lack of polymerization observed in the dark. Mechanistic studies involving luminescence changes, photolysis, cyclic voltammetry, and ESR spin trapping confirmed that the oxidative pathway predominantly drives the photopolymerization process. Additionally, the complex's exceptional performance in 3D direct laser writing (DLW) resins, tailored with three-component photoinitiating systems (PISs), demonstrated its suitability for advanced manufacturing applications. These findings position Mn(II) complexes as promising photocatalysts for photopolymerization and 3D printing technologies, offering a robust platform for future innovations in radical photoinitiating systems and functional materials development.

■ ASSOCIATED CONTENT

Supporting Information

The Supporting Information is available free of charge at https://pubs.acs.org/doi/10.1021/acsapm.5c00982.

Additional experimental procedure for Py-Imes synthesis, ^1H NMR and ^{13}C NMR spectra for py-Imes, UV−vis spectra, cyclic voltammetry, emission fluorescence spectra of MnPy-Imes, additional data about photocatalysts and additives, photolysis experiments, curves of SEC, and photopolymerization experiments (PDF)

■ AUTHOR INFORMATION

Corresponding Authors

Jacques Lalevée − *Université de Haute-Alsace, F-68100 Mulhouse, France;* orcid.org/0000-0001-9297-0335; Email: jacques.lalevee@uha.fr

Beatriz E. Goi − *School of Technology and Sciences, São Paulo State University (Unesp), Presidente Prudente, SP 19060-900, Brazil;* orcid.org/0000-0003-4369-7824; Email: beatriz.goi@unesp.br

Authors

Camila Bignardi − *School of Technology and Sciences, São Paulo State University (Unesp), Presidente Prudente, SP 19060-900, Brazil; Université de Haute-Alsace, F-68100 Mulhouse, France*

Naralyne M. Pesqueira − *School of Technology and Sciences, São Paulo State University (Unesp), Presidente Prudente, SP 19060-900, Brazil;* orcid.org/0000-0003-2581-9373

Yasmin M. Shimizo − *School of Technology and Sciences, São Paulo State University (Unesp), Presidente Prudente, SP 19060-900, Brazil*

Antonio E. H. Machado − *Instituto de Química, Universidade Federal de Uberlândia, Uberlândia 38400-089 Minas Gerais, Brazil*

Diesley M. S. Araújo − *Instituto Federal de Educação, Ciência e Tecnologia do Triângulo Mineiro, Ituiutaba 38305-200 Minas Gerais, Brazil;* orcid.org/0000-0002-5678-7821

Otaciro R. Nascimento − *Instituto de Física de São Carlos, Universidade de São Paulo, 13563-120 São Carlos, SP, Brazil*

https://doi.org/10.1021/acsapm.5c00982
ACS Appl. Polym. Mater. 2025, 7, 7429−7439

Valdemiro P. Carvalho, Jr. − *School of Technology and Sciences, São Paulo State University (Unesp), Presidente Prudente, SP 19060-900, Brazil*

Complete contact information is available at: https://pubs.acs.org/10.1021/acsapm.5c00982

Funding

The Article Processing Charge for the publication of this research was funded by the Coordenacao de Aperfeicoamento de Pessoal de Nivel Superior (CAPES), Brazil (ROR identifier: 00x0ma614).

Notes

The authors declare no competing financial interest.

■ ACKNOWLEDGMENTS

BEG, VPCJ, NMP, and CB are indebted to the financial support from FAPESP, grants #2021/11873-1, #2021/13128-1, #2021/11741-8, and #2022/16571-6, and #2024/03026-5, respectively, São Paulo Research Foundation (FAPESP). ORN thanks the financial support of CNPq (Process #308528/2023-9). The authors are grateful to Prof. Dra. Carla Cristina Schmitt Cavalheiro for the 400 MHz-NMR and MALDI-TOF performed at the Instituto de Química de São Carlos from Universidade de São Paulo. The authors are grateful to the Laboratório Multiusuário at São Paulo State University (Unesp), School of Technology and Sciences.

■ REFERENCES

(1) Hock, S. J.; Schaper, L.-A.; Herrmann, W. A.; Kühn, F. E. Group 7 Transition Metal Complexes with N-Heterocyclic Carbenes. *Chem. Soc. Rev.* **2013**, *42* (12), 5073.

(2) Wang, X.; He, J.; Wang, Y.-N.; Zhao, Z.; Jiang, K.; Yang, W.; Zhang, T.; Jia, S.; Zhong, K.; Niu, L.; Lan, Y. Strategies and Mechanisms of First-Row Transition Metal-Regulated Radical C−H Functionalization. *Chem. Rev.* **2024**, *124* (17), 10192−10280.

(3) Stroek, W.; Albrecht, M. Application of First-Row Transition Metal Complexes Bearing 1,2,3-Triazolylidene Ligands in Catalysis and Beyond. *Chem. Soc. Rev.* **2024**, *53* (12), 6322−6344.

(4) Liu, B.; Xia, Q.; Chen, W. Direct synthesis of iron, cobalt, nickel, and copper complexes of N-heterocyclic carbenes by using commercially available metal powders. *Angew. Chem. Weinheim Bergstr. Ger.* **2009**, *121* (30), 5621−5624.

(5) Qin, Y.; She, P.; Huang, X.; Huang, W.; Zhao, Q. Luminescent Manganese(II) Complexes: Synthesis, Properties and Optoelectronic Applications. *Coord. Chem. Rev.* **2020**, *416*, No. 213331.

(6) Vanden Broeck, S. M. P.; Cazin, C. S. J. Manganese-N-Heterocyclic Carbene (NHC) Complexes−An Overview. *Polyhedron* **2021**, *205*, No. 115204.

(7) Layfield, R. A. Manganese(II): The Black Sheep of the Organometallic Family. *Chem. Soc. Rev.* **2008**, *37* (6), 1098.

(8) Yao, Z.; Li, H.; Fan, Y.; Liang, X.; Xu, X.; Li, J. Pentacoordinated Cobalt(II) and Manganese(II) Porphyrin N-Heterocyclic Carbenes: Isolation, Characterization and Spectroscopy. *Dyes Pigm.* **2020**, *173* (107961), No. 107961.

(9) Al-Afyouni, M. H.; Krishnan, V. M.; Arman, H. D.; Tonzetich, Z. J. Synthesis and Reactivity of Manganese(II) Complexes Containing N-Heterocyclic Carbene Ligands. *Organometallics* **2015**, *34* (20), 5088−5094.

(10) Brousses, R.; Maurel, V.; Mouesca, J.-M.; César, V.; Lugan, N.; Valyaev, D. A. Half-Sandwich Manganese Complexes Cp(CO)2Mn-(NHC) as Redox-Active Organometallic Fragments. *Dalton Trans.* **2021**, *50* (40), 14264−14272.

(11) Hockin, B. M.; Li, C.; Robertson, N.; Zysman-Colman, E. Photoredox Catalysts Based on Earth-Abundant Metal Complexes. *Catal. Sci. Technol.* **2019**, *9* (4), 889−915.

(12) Tao, P.; Liu, S.-J.; Wong, W.-Y. Phosphorescent Manganese(II) Complexes and Their Emerging Applications. *Adv. Opt. Mater.* **2020**, *8* (20), 2000985.

(13) Cahiez, G.; Duplais, C.; Buendia, J. Chemistry of Organomanganese(II) Compounds. *Chem. Rev.* **2009**, *109* (3), 1434−1476.

(14) Huang, S.; Hong, X.; Cui, H.-Z.; Zhan, B.; Li, Z.-M.; Hou, X.-F. Bimetallic Bis-NHC-Ir(III) Complex Bearing 2-Arylbenzo[*d*]Oxazolyl Ligand: Synthesis, Catalysis, and Bimetallic Effects. *Organometallics* **2020**, *39* (19), 3514−3523.

(15) Visbal, R.; Gimeno, M. C. N-Heterocyclic Carbene Metal Complexes: Photoluminescence and Applications. *Chem. Soc. Rev.* **2014**, *43* (10), 3551−3574.

(16) Khramov, D. M.; Lynch, V. M.; Bielawski, C. W. N-heterocyclic carbene - Transition metal complexes: Spectroscopic and crystallographic analyses of π-Back-bonding Interactions. *Organometallics* **2007**, *26* (24), 6042−6049.

(17) Pinaud, J.; Trinh, T. K. H.; Sauvanier, D.; Placet, E.; Songsee, S.; Lacroix-Desmazes, P.; Becht, J.-M.; Tarablsi, B.; Lalevée, J.; Pichavant, L.; Héroguez, V.; Chemtob, A. In Situ Generated Ruthenium-Arene Catalyst for Photoactivated Ring-Opening Metathesis Polymerization through Photolatent N-Heterocyclic Carbene Ligand. *Chemistry* **2018**, *24* (2), 337−341.

(18) Poland, E. M.; Ho, C. C. Photoactive *N*-heterocyclic Carbene Transition Metal Complexes in Bond-forming Photocatalysis: State-of-the-art and Opportunities. *Appl. Organomet. Chem.* **2024**, *38* (10), No. e6746.

(19) Figueiredo, M. L. B.; Bignardi, C.; Pesqueira, N. M.; Machado, A. E. H.; Carvalho, V. P., Jr.; Nascimento, O. R.; Goi, B. E. Well-Defined Non-Symmetric NHC-Iron(III) Catalyst for Photoinduced Atom-Transfer Radical Polymerization of Methyl Methacrylate. *J. Photochem. Photobiol. A Chem.* **2024**, *452* (115567), No. 115567.

(20) Lalevée, J.; Lacôte, E.; Telitel, S.; Blanchard, N.; Graff, B. Homolytic Photocleavage of the B−N Bond in N-Heterocyclic Carbene Borane Scaffolds: Towards Efficient Type I Photoinitiators. *Synthesis (Mass.)* **2025**, *57*, A−F.

(21) Pesqueira, N. M.; Morlet-Savary, F.; Schmitt, M.; Carvalho, V. P.; Goi, B. E.; Lalevée, J. Visible Light-Promoted Nickel-NHC Photocatalysts for Free Radical Photopolymerization and 3D Printing Application. *Poly.Chem.* **2025**, *16*, 2436−2448.

(22) Amouri, H. Luminescent Complexes of Platinum, Iridium, and Coinage Metals Containing N-Heterocyclic Carbene Ligands: Design, Structural Diversity, and Photophysical Properties. *Chem. Rev.* **2023**, *123* (1), 230−270.

(23) Mondal, A.; Sahu, P.; Kisan, H. K.; Isab, A. A.; Chandra, S. K.; Dinda, J. Dinuclear Silver(I)- and Gold(I)- N Heterocyclic Carbene Complexes; Synthesis, Structural Characterizations, Photoluminescence and Theoretical Studies. *J. Mol. Struct.* **2023**, *1274*, No. 134430.

(24) Jhulki, L.; Purkait, R.; Kisan, H.; Bertolasi, V.; Isab, A.; Sinha, C.; Dinda, J. A Promising Class of Luminescent Derivatives of Silver(I) and Gold(I)- N -heterocyclic Carbene. *Appl. Organomet. Chem.* **2020**, *34* (8), DOI: 10.1002/aoc.5673.

(25) Idris, M.; Kapper, S. C.; Tadle, A. C.; Batagoda, T.; Muthiah Ravinson, D. S.; Abimbola, O.; Djurovich, P. I.; Kim, J.; Coburn, C.; Forrest, S. R.; Thompson, M. E. Blue Emissive Fac/Mer -Iridium (III) NHC Carbene Complexes and Their Application in OLEDs. *Adv. Opt. Mater.* **2021**, *9* (8), 2001994.

(26) Mackenzie, C. F. R.; Zhang, L.; Cordes, D. B.; Slawin, A. M. Z.; Samuel, I. D. W.; Zysman-Colman, E. Bulky Iridium NHC Complexes for Bright, Efficient Deep-blue OLEDs. *Adv. Opt. Mater.* **2023**, *11* (2), 2201495.

(27) Ryan, R. T.; Stevens, K. C.; Calabro, R.; Parkin, S.; Mahmoud, J.; Kim, D. Y.; Heidary, D. K.; Glazer, E. C.; Selegue, J. P. Bis-Tridentate N-Heterocyclic Carbene Ru(II) Complexes Are Promising New Agents for Photodynamic Therapy. *Inorg. Chem.* **2020**, *59* (13), 8882−8892.

(28) Villani, E.; Sakanoue, K.; Einaga, Y.; Inagi, S.; Fiorani, A. Photophysics and Electrochemistry of Ruthenium Complexes for

Electrogenerated Chemiluminescence. *J. Electroanal. Chem. (Lausanne Switz)* **2022**, *921* (116677), No. 116677.
(29) Lu, Y.; Wang, J.; Wu, Y.; Xu, S.; Zhao, F.; He, H.; Wang, Y. Yellow−Green Luminescence of Four-Coordinate Copper(I) Complexes Bearing N−Heterocyclic Carbene (NHC) Ligands: Synthesis, Photophysical and Computational Studies. *Polyhedron* **2021**, *210* (115500), No. 115500.
(30) Schmeinck, P.; Sretenovic, D.; Guhl, J.; Kühnemuth, R.; Seidel, C. A. M.; Marian, C. M.; Suta, M.; Ganter, C. Luminescent Copper(I)-Complexes with an Anionic NHC Obtained via a Coordination Polymer as Versatile Precursor. *ChemRxiv* **2023**, *26* (27), No. e202300416.
(31) Chen, H.; Zhang, Y.; Bonfiglio, A.; Morlet-Savary, F.; Mauro, M.; Lalevée, J. Rhenium(I) N-Heterocyclic Carbene Complexes in Photoinitiating Systems for Polymerization upon Visible Light: Development of Photosensitive Resins for 3D and 4D Applications. *ACS Appl. Polym. Mater.* **2021**, *3* (1), 464−473.
(32) Bonfiglio, A.; Magra, K.; Cebrián, C.; Polo, F.; Gros, P. C.; Mercandelli, P.; Mauro, M. Red-Emitting Neutral Rhenium(i) Complexes Bearing a Pyridyl Pyridoannelated N-Heterocyclic Carbene. *Dalton Trans.* **2020**, *49* (10), 3102−3111.
(33) Telitel, S.; Dumur, F.; Campolo, D.; Poly, J.; Gigmes, D.; Pierre Fouassier, J.; Lalevée, J. Iron Complexes as Potential Photocatalysts for Controlled Radical Photopolymerizations: A Tool for Modifications and Patterning of Surfaces. *J. Polym. Sci. A Polym. Chem.* **2016**, *54* (5), 702−713.
(34) Zhang, H.; Liu, J.; Chen, J.; Zhao, J.; Zhao, Y.; Li, L. A Modified Procedure for the Synthesis of 1-Arylimidazoles. *Synthesis (Mass.)* **2003**, *17*, 2661−2666.
(35) Warsink, S.; Chang, I.-H.; Weigand, J. J.; Hauwert, P.; Chen, J.-T.; Elsevier, C. J. NHC Ligands with a Secondary Pyrimidyl Donor for Electron-Rich Palladium(0) Complexes. *Organometallics* **2010**, *29* (20), 4555−4561.
(36) Chai, J.; Zhu, H.; Peng, Y.; Roesky, H. W.; Singh, S.; Schmidt, H.-G.; Noltemeyer, M. Synthesis and Structural Characterization of Monomeric Manganese(II) *N*-heterocyclic Carbene Complexes $[MnX_2(CN(ipr)C(Me)_2)_2]$ (X = Cl, I, and MeCOO). *Eur. J. Inorg. Chem.* **2004**, *13*, 2673−2677.
(37) Schlagintweit, J. F.; Altmann, P. J.; Böth, A. D.; Hofmann, B. J.; Jandl, C.; Kaußler, C.; Nguyen, L.; Reich, R. M.; Pöthig, A.; Kühn, F. E. Activation of Molecular Oxygen by a Cobalt(II) tetra-NHC Complex. *Chemistry* **2021**, *27* (4), 1311−1315.
(38) Magra, K.; Francés-Monerris, A.; Cebrián, C.; Monari, A.; Haacke, S.; Gros, P. C. Bidentate pyridyl-NHC Ligands: Synthesis, Ground and Excited State Properties of Their Iron(II) Complexes and the Role of the Fac/Mer Isomerism. *Eur. J. Inorg. Chem.* **2022**, *2022* (7), No. e202100818.
(39) Yao, Z.; Li, H.; Fan, Y.; Liang, X.; Xu, X.; Li, J. Pentacoordinated Cobalt(II) and Manganese(II) Porphyrin N-Heterocyclic Carbenes: Isolation, Characterization and Spectroscopy. *Dyes Pigm.* **2020**, *173* (107961), No. 107961.
(40) Lakshmi, D. S.; Cundari, T.; Furia, E.; Tagarelli, A.; Fiorani, G.; Carraro, M.; Figoli, A. Preparation of Polymeric Membranes and Microcapsules Using an Ionic Liquid as Morphology Control Additive. *Macromol. Symp.* **2015**, *357* (1), 159−167.
(41) Refat, M. S.; Ibrahim, H. K.; Sowellim, S. Z. A.; Soliman, M. H.; Saeed, E. M. Spectroscopic and Thermal Studies of Mn(II), Fe(III), Cr(III) and Zn(II) Complexes Derived from the Ligand Resulted by the Reaction between 4-Acetyl Pyridine and Thiosemicarbazide. *J. Inorg. Organomet. Polym. Mater.* **2009**, *19* (4), 521−531.
(42) Banerjee, S.; Ghorai, P.; Sarkar, P.; Panja, A.; Saha, A. A Rare Flattened Tetrahedral Mn(II) Salen Type Complex: Synthesis, Crystal Structure, Biomimetic Catalysis and DFT Study. *Inorg. Chim. Acta* **2020**, *499* (119176), No. 119176.
(43) Zhao, Y.; Truhlar, D. G. The M06 Suite of Density Functionals for Main Group Thermochemistry, Thermochemical Kinetics, Noncovalent Interactions, Excited States, and Transition Elements: Two New Functionals and Systematic Testing of Four M06-Class Functionals and 12 Other Functionals. *Theor. Chem. Acc.* **2008**, *120* (1−3), 215−241.
(44) Jorge, F. E.; Canal Neto, A.; Camiletti, G. G.; Machado, S. F. Contracted Gaussian Basis Sets for Douglas-Kroll-Hess Calculations: Estimating Scalar Relativistic Effects of Some Atomic and Molecular Properties. *J. Chem. Phys.* **2009**, *130* (6), No. 064108.
(45) Pritchard, B. P.; Altarawy, D.; Didier, B.; Gibson, T. D.; Windus, T. L. New Basis Set Exchange: An Open, up-to-Date Resource for the Molecular Sciences Community. *J. Chem. Inf. Model.* **2019**, *59* (11), 4814−4820.
(46) Barone, V.; Cossi, M. Quantum Calculation of Molecular Energies and Energy Gradients in Solution by a Conductor Solvent Model. *J. Phys. Chem. A* **1998**, *102* (11), 1995−2001.
(47) Cossi, M.; Rega, N.; Scalmani, G.; Barone, V. Energies, Structures, and Electronic Properties of Molecules in Solution with the C-PCM Solvation Model. *J. Comput. Chem.* **2003**, *24* (6), 669−681.
(48) Ivanov, V.; Trostianko, P.; Kovalenko, S.; Volodchenko, A.; Chernozhuk, T.; Stepaniuk, D.; Kalugin, O. Quantum-Chemical Calculations of Electronic Spectra Absorption: Ab Initio or Semi-empirical Methods? *Kharkov Univ. Bull. Chem. Ser.* **2021**, *36*, 33−43.
(49) Frisch, M. J.; Trucks, G. W.; Schlegel, H. B.; Scuseria, G. E.; Robb, M. A.; Cheeseman, J. R.; Scalmani, G.; Barone, V.; Mennucci, B.; Petersson, G. A.; Nakatsuji, H.; Caricato, M.; Li, X.; Hratchian, H. P.; Izmaylov, A. F.; Bloino, J.; Zheng, G.; Sonnenberg, J. L.; Hada, M.; Ehara, M.; Toyota, K.; Fukuda, R.; Hasegawa, J.; Ishida, M.; Nakajima, T.; Honda, Y.; Kitao, O.; Nakai, H.; Vreven, T.; Montgomery, J. A., Jr.; Peralta, J. E.; Ogliaro, F.; Bearpark, M.; Heyd, J. J.; Brothers, E.; Kudin, K. N.; Staroverov, V. N.; Keith, T.; Kobayashi, R.; Normand, J.; Raghavachari, K.; Rendell, A.; Burant, J. C.; Iyengar, S. S.; Tomasi, J.; Cossi, M.; Rega, N.; Millam, J. M.; Klene, M.; Knox, J. E.; Cross, J. B.; Bakken, V.; Adamo, C.; Jaramillo, J.; Gomperts, R.; Stratmann, R. E.; Yazyev, O.; Austin, A. J.; Cammi, R.; Pomelli, C.; Ochterski, J. W.; Martin, R. L.; Morokuma, K.; Zakrzewski, V. G.; Voth, G. A.; Salvador, P.; Dannenberg, J. J.; Dapprich, S.; Daniels, A. D.; Farkas, O.; Foresman, J. B.; Ortiz, J. V.; Cioslowski, J.; Fox, D. J. *Gaussian 09*, Revision E.01; Gaussian, Inc., Wallingford, CT, 2013.
(50) Shotonwa, I. O.; Kpomah, B.; Durodola, B. M.; Adesoji, A. O.; Plass, W.; Adewuyi, S. Electrocatalytic Reduction of Protons with Bis(N-Para-Carboxyphenyldithiocarbamato)-(1,10-Phenanthroline) Cobalt(II) and Manganese(II) Complexes. *J. Electroanal. Chem. (Lausanne Switz)* **2024**, *973* (118664), No. 118664.
(51) Hou, C.-L.; Song, J.-X.; Chang, X.; Chen, Y. Photoluminescent Nickel(II) Carbene Complexes with Ligand-to-Ligand Charge-Transfer Excited States. *Chin. Chem. Lett.* **2024**, *35* (1), No. 108333.
(52) Garra, P.; Morlet-Savary, F.; Dietlin, C.; Fouassier, J.-P.; Lalevée, J. Charge-Transfer Complexes as New Inhibitors/Photoinitiators for on-Demand Amine/Peroxide Redox Polymerization. *ACS Omega* **2018**, *3* (6), 6827−6832.
(53) Garra, P.; Morlet-Savary, F.; Dietlin, C.; Fouassier, J. P.; Lalevée, J. On-Demand Visible Light Activated Amine/Benzoyl Peroxide Redox Initiating Systems: A Unique Tool to Overcome the Shadow Areas in Photopolymerization Processes. *Macromolecules* **2016**, *49* (24), 9371−9381.
(54) Pesqueira, N. M.; Morlet-Savary, F.; Schmitt, M.; Carvalho, V. P., Jr.; Goi, B. E.; Lalevée, J. Advancing Photopolymerization and 3D Printing: High-Performance NiII Complexes Bearing N2O2 Schiff-Base Ligands as Photocatalysts. *Eur. Polym. J.* **2024**, *216* (113279), No. 113279.
(55) Lang, M.; Hirner, S.; Wiesbrock, F.; Fuchs, P. A Review on Modeling Cure Kinetics and Mechanisms of Photopolymerization. *Polymers (Basel)* **2022**, *14* (10), 2074.
(56) Pesqueira, N. M.; Morlet-Savary, F.; Schmitt, M.; Jouaiti, A.; Goi, B. E.; Mauro, M.; Lalevée, J. Heteroleptic Copper(I) Complexes with Pyridine-Benzothiazole Ligands as Photocatalysts for Free Radical Photopolymerization and 3D Printing. *ACS Appl. Polym. Mater.* **2025**, *7*, 2615−2623.

https://doi.org/10.1021/acsapm.5c00982
ACS Appl. Polym. Mater. 2025, 7, 7429−7439

(57) Dumur, F.; Lalevée, J. Recent Advances in Photoredox Catalysts. *Catalysts* **2024**, *14* (1), 26.
(58) Mtshali, Z.; von Eschwege, K. G.; Conradie, J. Electrochemical Study of the Mn(II/III) Oxidation of Tris(Polypyridine)Manganese-(II) Complexes. *Electrochim. Acta* **2021**, *391* (138965), No. 138965.
(59) Tar, H.; Kashar, T. I.; Kouki, N.; Aldawas, R.; Graff, B.; Lalevée, J. Novel Copper Photoredox Catalysts for Polymerization: An in Situ Synthesis of Metal Nanoparticles. *Polymers (Basel)* **2020**, *12* (10), 2293.

https://doi.org/10.1021/acsapm.5c00982
ACS Appl. Polym. Mater. 2025, 7, 7429−7439